Geoeffectiveness (*Dst* and *Kp*) of interplanetary coronal mass ejections during 1995–2009 and implications for storm forecasting

I. G. Richardson[1,2] and H. V. Cane[1,3]

Received 22 February 2011; revised 5 April 2011; accepted 20 April 2011; published 21 July 2011.

[1] We summarize the geoeffectiveness (based on the *Dst* and *Kp* indices) of the more than 300 interplanetary coronal mass ejections (ICMEs) that passed the Earth during 1996–2009, encompassing solar cycle 23. We subsequently estimate the probability that an ICME will generate geomagnetic activity that exceeds certain thresholds of *Dst* or *Kp*, including the NOAA "G" storm scale, based on maximum values of the southward magnetic field component (B_s), the solar wind speed (V), and the y component (E_y) of the solar wind convective electric field $E = -V \times B$, in the ICME or sheath ahead of the ICME. Consistent with previous studies, the geoeffectiveness of an ICME is correlated with B_s or $E_y \approx VB_s$ in the ICME or sheath, indicating that observations from a solar wind monitor upstream of the Earth are likely to provide the most reliable forecasts of the activity associated with an approaching ICME. There is also a general increase in geoeffectiveness with ICME speed, though the overall event-to-event correlation is weaker than for B_s and E_y. Nevertheless, using these results, we suggest that the speed of an ICME approaching the Earth inferred, for example, from routine remote sensing by coronagraphs on spacecraft well separated from the Earth or by all-sky imagers, could be used to estimate the likely geoeffectiveness of the ICME (our "comprehensive" ICME database provides a proxy for ICMEs identified in this way) with a longer lead time than may be possible using an upstream monitor.

Citation: Richardson, I. G., and H. V. Cane (2011), Geoeffectiveness (*Dst* and *Kp*) of interplanetary coronal mass ejections during 1995–2009 and implications for storm forecasting, *Space Weather*, *9*, S07005, doi:10.1029/2011SW000670.

1. Introduction

[2] Interplanetary coronal mass ejections (ICMEs), the interplanetary manifestations of coronal mass ejections at the Sun, are well known to be important drivers of enhanced geomagnetic activity including geomagnetic storms [e.g., *Zhang and Burlaga*, 1988; *Gosling et al.*, 1991; *Tsurutani and Gonzalez*, 1997; *Richardson et al.*, 2001; *Huttunen and Koskinen*, 2004; *Huttunen et al.*, 2005; *Zhang et al.*, 2007; *Wu and Lepping*, 2007; *Echer et al.*, 2008, and references therein]. Recently [*Richardson and Cane*, 2010], we compiled a "comprehensive" catalog of the 340 ICMEs that passed the Earth in 1996–2009, a period encompassing solar cycle 23, that extends and updates our previous catalog of events in 1996–2002 [*Cane and Richardson*, 2003]. In this paper, we summarize how the probability of exceeding certain geomagnetic activity thresholds, as indicated by the *Dst* [*Sugiura*, 1964; *Rostoker*, 1972; *Mayaud*, 1980] and *Kp* [*Bartels et al.*, 1939; *Rostoker*, 1972; *Mayaud*, 1980; *Menvielle and Berthelier*, 1991] indices, varies with the solar wind parameters of the ICME and upstream sheath for this large sample of events. In particular, we consider whether the ICME speed can be used as an indicator of potential geoeffectiveness, a primary motivation being that, using remote sensing for example by coronagraphs on the STEREO spacecraft separated in heliolongitude from the Earth or all sky imagers such as the Solar Mass Ejection Imager, it is now possible to identify ICMEs moving out in the direction of the Earth [e.g., *Howard et al.*, 2006; *Webb et al.*, 2006; *Davis et al.*, 2009; *Thernisien et al.*, 2009; *Liu et al.*, 2010; *Davis et al.*, 2011]. Our "comprehensive" ICME database provides a proxy for the situation when routine monitoring is able to identify most, if not all of the ICMEs approaching the Earth and measure their speeds.

[3] The identification of the ICMEs used in this study is discussed by *Cane and Richardson* [2003] and *Richardson and Cane* [2010, and references therein] and makes use of a number of the characteristic in situ signatures of ICMEs

[1]Astroparticle Physics Laboratory, NASA Goddard Space Flight Center, Greenbelt, Maryland, USA.
[2]CRESST and Department of Astronomy, University of Maryland, College Park, Maryland, USA.
[3]School of Mathematics and Physics, University of Tasmania, Hobart, Tasmania, Australia.

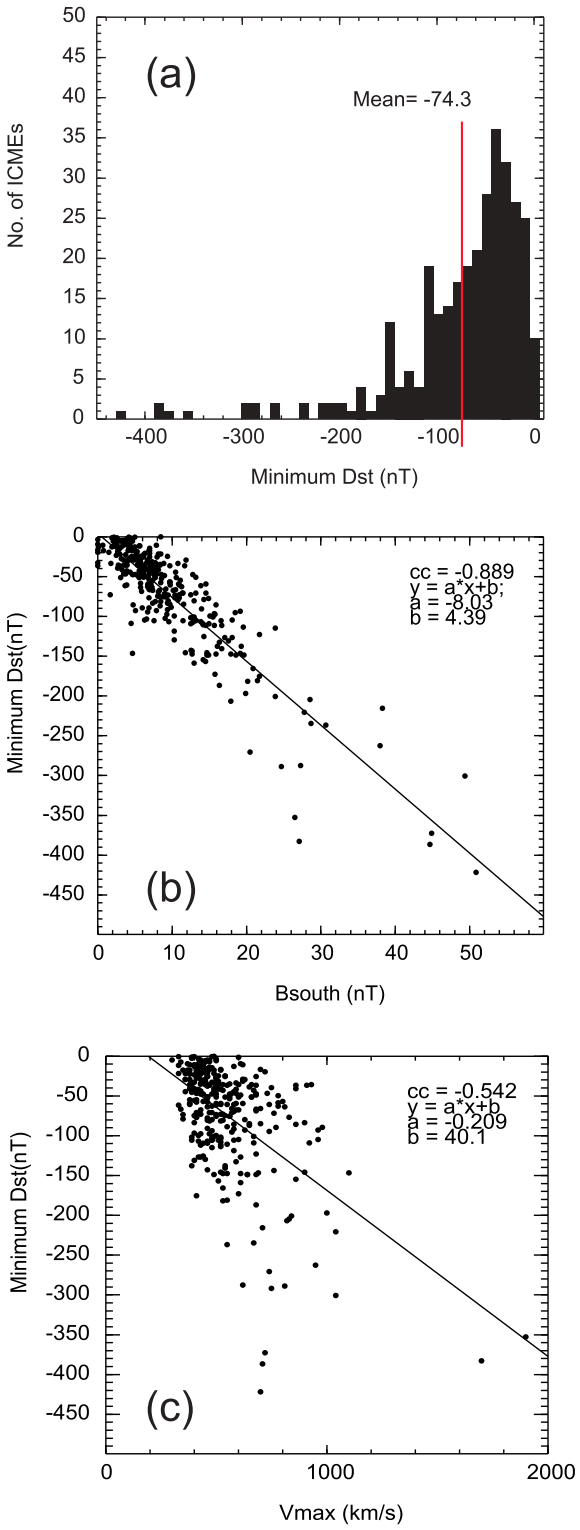

Figure 1. (a) Distribution of minimum *Dst* during the passage of the ICMEs in 1996–2009 and their associated sheath regions. Minimum *Dst* associated with passage of the ICME or upstream sheath versus maximum 1 hour averaged (b) B_s or (c) solar wind speed.

(see reviews by *Gosling* [1990], *Neugebauer and Goldstein* [1997], and *Zurbuchen and Richardson* [2006]). The ICME catalog of *Richardson and Cane* [2010] includes the estimated times of passage of the leading and trailing edges of the ICMEs and of the associated shock driven by the ICME, if present, which occurs several hours ahead of arrival of the ICME. The region between the shock and the ICME leading edge is termed the "sheath." In the case of slower ICMEs, the shock may be weak, developing or absent. For sample events illustrating the relationship between near-Earth solar wind parameters and geomagnetic activity during the passage of ICMEs, see for example, *Gonzalez and Tsurutani* [1987], *Tsurutani and Gonzalez* [1997], *Farrugia et al.* [1998], *Huttunen et al.* [2005], *Zhang et al.* [2007, 2008], *Richardson and Zhang* [2008], and *Echer et al.* [2008].

2. Results

2.1. *Dst* Index During the Passage of ICMEs

[4] Figure 1a shows the distribution of minimum *Dst* measured during the passage of the ICMEs in 1996–2009 cataloged by *Richardson and Cane* [2010] or their associated sheath regions. (Both ICMEs and sheaths may contribute to the geomagnetic activity [e.g., *Tsurutani et al.*, 1988; *Huttunen and Koskinen*, 2004; *Huttunen et al.*, 2005; *Zhang et al.*, 2007].) The mean minimum value of *Dst* is –74.3 nT while the most probable minimum value is ~–40 nT. Some 25% of the events have *Dst* ≤ –100 nT, i.e., were associated with an "intense" storm [*Tsurutani and Gonzalez*, 1997]. There is also an extended tail of events associated with exceptionally high levels of geomagnetic activity. In particular, 6% of the ICMEs were associated with "severe" storms (*Dst* ≤ –200 nT [*Tsurutani and Gonzalez*, 1997]). Thus, although ICMEs are widely recognized as important drivers of the largest geomagnetic storms, clearly only a small subset of the cycle 23 ICMEs (or associated sheaths) gave rise to such storms.

[5] Note that the *Dst* values used here are "final" values to 2003, "provisional" values for 2004–2007, and "quick-look" values thereafter, obtained from the WDC for Geomagnetism, Kyoto (http://wdc.kugi.kyoto-u.ac.jp/). The provisional and quick-look values may be subject to future revision (typically by only a few nT), but the main conclusions of this paper should not be affected. In addition, we have not included in the analysis seven ICMEs for which geomagnetic activity was dominated by ongoing activity from a previous event.

[6] Why should ICMEs display such a wide range of geoeffectiveness? It is well known that enhanced geoeffectiveness is associated with intervals of increased southward solar wind magnetic field and the y component of the electric field [e.g., *Tsurutani and Gonzalez*, 1997, and references therein] which drive enhanced reconnection with the magnetospheric magnetic fields [*Dungey*, 1961]. Figure 1b shows minimum *Dst* plotted versus the maximum southward magnetic field component (B_s, in GSM coordinates) during passage of the sheath or ICME based on 1 hour averages of observations from near-Earth spacecraft and is consistent with this view. (The observations are from the

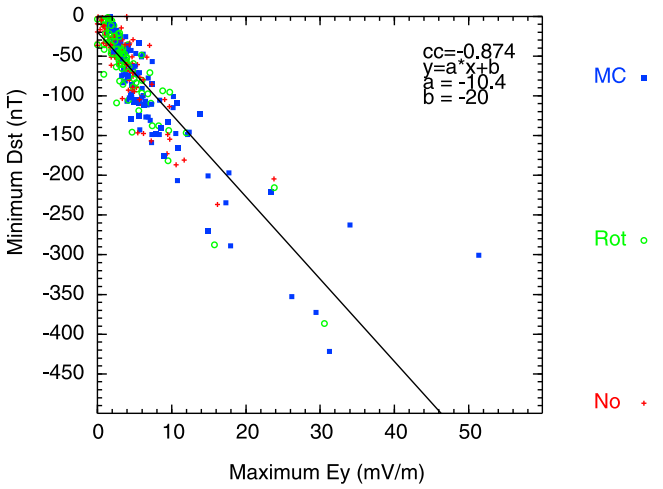

Figure 2. Minimum *Dst* plotted versus maximum E_y for ICMEs in 1996–2009. Blue symbols indicate ICMEs that are magnetic clouds, green symbols indicate those that include a magnetic field rotation but do not meet the criteria for magnetic clouds, and red symbols indicate those ICMEs without an organized, flux-rope-like magnetic field.

OMNI database and from individual spacecraft including ACE and WIND. There are a few minor corrections compared with Figure 14 of *Richardson and Cane* [2010].) The correlation coefficient (*cc*) is –0.889, and the best fit line gives a relationship $Dst = -8.03B_s + 4.39$, where *Dst* and B_s are in nT. Note that this relationship extends down to the weakest storms. There is a much poorer correlation between minimum *Dst* and the solar wind speed (Figure 1c), where we use the maximum solar wind speed observed in the sheath or ICME. The correlation (*cc* = –0.542) is largely determined by two fast ICMEs associated with severe storms. A caveat to these results is that in situ solar wind speed measurements are not complete for a few of the faster ICMEs. The relationship between ICME parameters and geoeffectiveness has also been discussed by, for example, *Kane* [2005] and *Gopalswamy et al.* [2008] (for magnetic clouds).

[7] Figure 2 shows minimum *Dst* plotted versus the maximum value of E_y, the (GSM) y component of the solar wind convective electric field $E = -V \times B$ (i.e., $E_y \approx VB_s$), in the sheath or ICME, again based on 1 hour averages. The correlation coefficient is –0.874. The relationship between minimum *Dst* and E_y is given by $Dst = -10.4E_y - 20.0$, where E_y is in mV/m. The symbol indicates the magnetic field configuration of the ICME based on the work of *Richardson and Cane* [2010]. A blue square indicates a magnetic cloud, an ICME including an enhanced magnetic field >10 nT with a smooth rotation in field through a large angle suggestive of a flux-rope-like magnetic field configuration [e.g., *Klein and Burlaga*, 1982; *Lepping et al.*, 2006] corresponding to the "class 2" events of *Richardson and Cane* [2010]. A green circle indicates evidence of a field rotation but the other criteria for a magnetic cloud (such as the enhanced magnetic field intensity) were not met ("class 1" events), while a red cross indicates that the field shows no evidence of a rotation or an organized magnetic field ("class 0" events). It is clear that the majority of the most geoeffective ICMEs were those with magnetic cloud signatures (see, e.g., *Farrugia et al.* [1997] for a discussion of the geomagnetic response to magnetic clouds). In particular, 61% of the ICMEs associated with severe ($Dst \le -200$ nT) storms were magnetic clouds, as were a similar fraction of the ICMEs associated with $-200 \le Dst \le -100$ nT storms. Weaker activity levels were predominantly associated with non-cloud ICMEs [see also *Wu and Lepping*, 2007]. For example, only 22% of ICMEs associated with minimum $Dst > -50$ nT were magnetic clouds while 41% had no rotation or organized magnetic field. Overall, around 48% of magnetic clouds during 1996–2009 were associated with intense or stronger storms, and 11% with severe storms.

[8] We now consider how the probability of generating an intense or severe storm varies with the maximum value of E_y or B_s in the ICME or sheath as might be measured by a monitor upstream of the Earth. Considering E_y, Figure 3 shows the probability of an ICME or sheath producing activity with $Dst \le -50$ nT, ≤–100 nT (intense storm), ≤–150 nT, ≤–200 nT (severe storm) and ≤–300 nT as a function of maximum E_y. For example, for $E_y < 4$ mV/m, there is only a small probability of an intense storm being

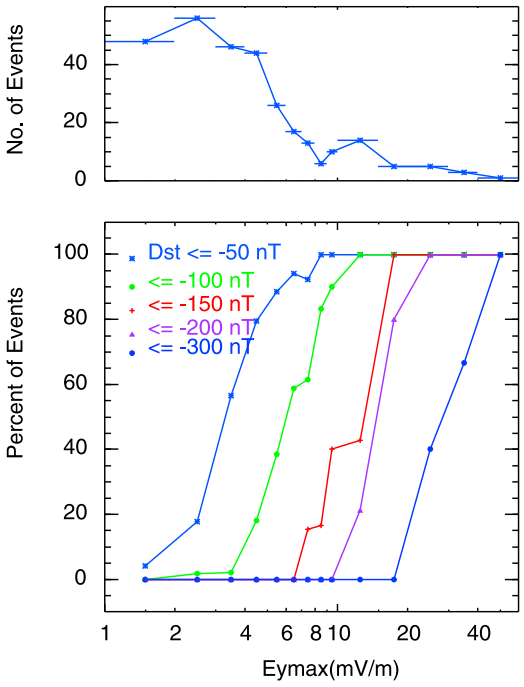

Figure 3. (top and bottom) Variation of the percentage of events with $Dst \le -50$ nT, ≤–100 nT, ≤–150 nT, ≤–200 nT, and ≤–300 nT versus maximum E_y in the ICME or sheath. The number of events in each E_y range is shown in Figure 3 (top).

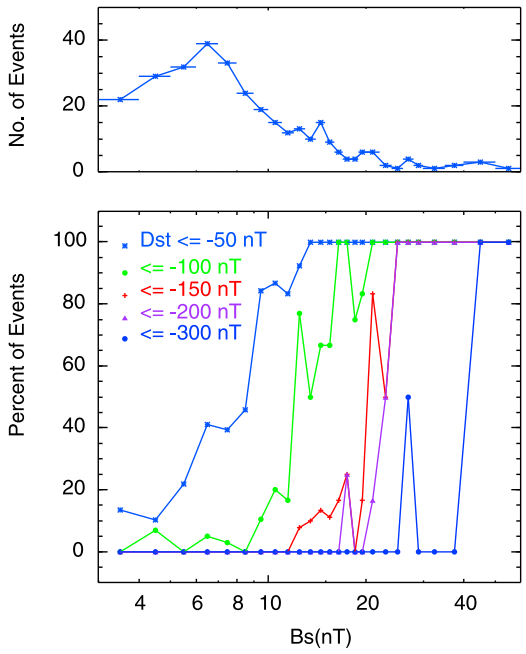

Figure 4. (top and bottom) Variation of the probability of minimum *Dst* exceeding thresholds ranging from −50 nT to −300 nT versus maximum B_s in the ICME or sheath. Figure 4 (top) shows the number of events in each B_s range.

generated, while for $E_y \geq 10$ mV/m, all ICMEs are associated with intense storms. A 50% probability of an intense storm occurs at $E_y \sim 6$ mV/m. This result is consistent with those of previous studies. For example, *Gonzalez and Tsurutani* [1987] concluded that $E_y > 5$ mV/m for a duration of >3 hours is required to generate an intense storm (a similar result was found by *Echer et al.* [2008] for the cycle 23 intense storms) although *Farrugia et al.* [1998] noted a similar situation that was not accompanied by an intense storm. (Though we have not considered the duration of enhanced values of E_y specifically in our analysis, the use of 1 hour averaged values requires that these conditions persist for durations of this order.) *Ji et al.* [2010] concluded that $E_y \geq 5$ mV/m for ≥2 hours was a "promising candidate" to trigger an intense storm, again based on the cycle 23 events. Returning to Figure 3, severe storms require $E_y > 10$ mV/m, and all ICMEs or sheaths with $E_y > 20$ mV/m produced such storms. The 50% probability point is estimated to be $E_y \sim 15$ mV/m. For a $Dst \leq -50$ nT ICME-associated storm, 50% probability is at ~3 mV/m. Figure 3 (top) shows the number of ICMEs included in each range of E_y. Although there is an excellent sampling of events for the weaker activity levels, note that the conclusions regarding the conditions leading to the strongest storms are based on small numbers of events.

[9] Considering B_s in a similar way (Figure 4), intense storms are rarely associated with ICMEs or upstream sheaths with $B_s < 10$ nT, while most cases with $B_s \geq 16$ nT are associated with such storms; 50% probability is at $B_s \sim 12$ nT.

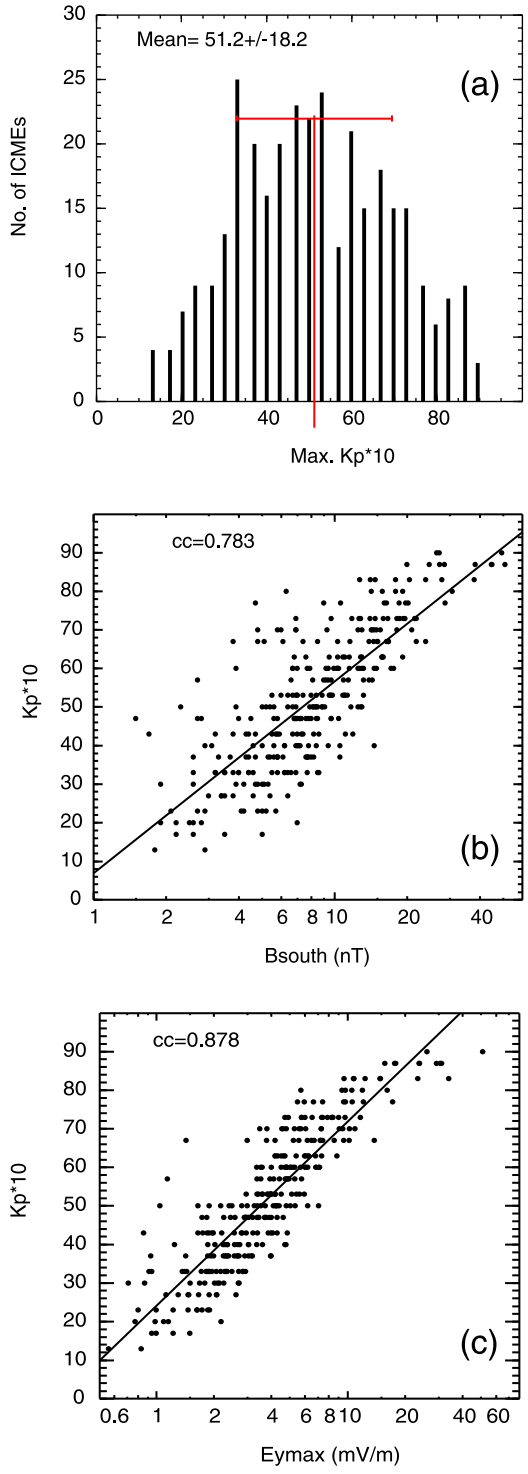

Figure 5. (a) Distribution of maximum *Kp**10 values for the 1996–2009 ICMEs. Maximum *Kp**10 values versus maximum 1 hour averaged value of (b) B_s or (c) E_y.

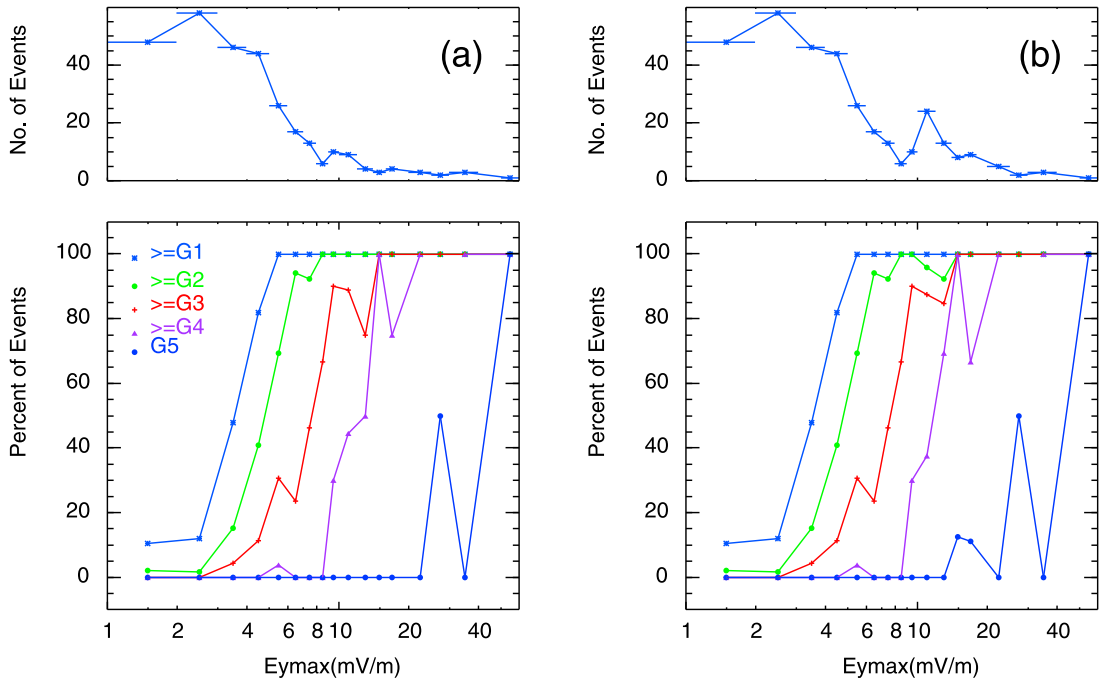

Figure 6. (a and b) Probability of storms equaling or exceeding NOAA sizes G1 to G5 versus maximum E_y in the ICME or sheath. Figure 6b includes 34 pre-1996 events with $E_y \geq 10$ mV/m.

This is comparable to the condition $B_z < -10$ nT for >3 hours for the drivers of intense storms noted by *Gonzalez and Tsurutani* [1987] and by *Ji et al.* [2010] (who additionally suggest the condition $B_z < -15$ nT for >2 hours). Severe storms are rarely associated with $B_s < 20$ nT, but all events with $B_s \geq 23$ nT produced such storms, though again we note that these conclusions are based on a small sample of events.

2.2. *Kp*

[10] We now turn to consider the behavior of the *Kp* geomagnetic index during the passage of the cycle 23 ICMEs and the associated sheaths. Figure 5a shows the distribution of maximum *Kp**10 (where *Kp**10 = 7 corresponds to $Kp = 1^-$; *Kp**10 = 10 corresponds to *Kp* = 1; *Kp**10 = 13 corresponds to $Kp = 1^+$, etc). The mean maximum value of *Kp**10 is 51.2, i.e., *Kp* ~ 5. The broad distribution again emphasizes that ICMEs are associated with a range of geoeffectiveness. Figures 5b and 5c show correlations between maximum *Kp**10 and maximum B_s (*cc* = 0.783) or E_y (*cc* = 0.878), respectively.

[11] In Figure 6 we show the probability of generating storms equaling or exceeding the NOAA "G" storm sizes (http://www.swpc.noaa.gov/NOAAscales/) that are based

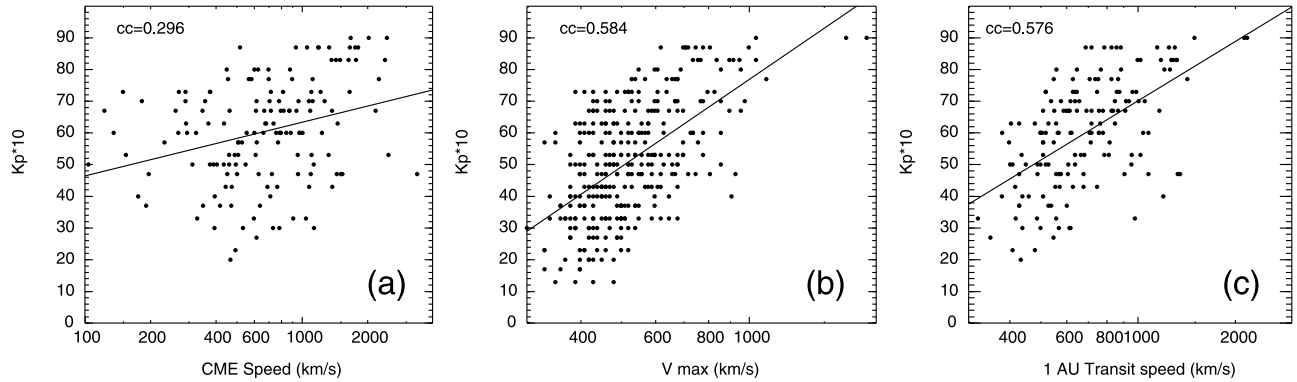

Figure 7. Maximum *Kp**10 plotted versus (a) the plane of the sky speed of the associated LASCO halo or partial halo CME, (b) the maximum solar wind speed in the ICME or sheath, and (c) the disturbance 1 AU transit speed.

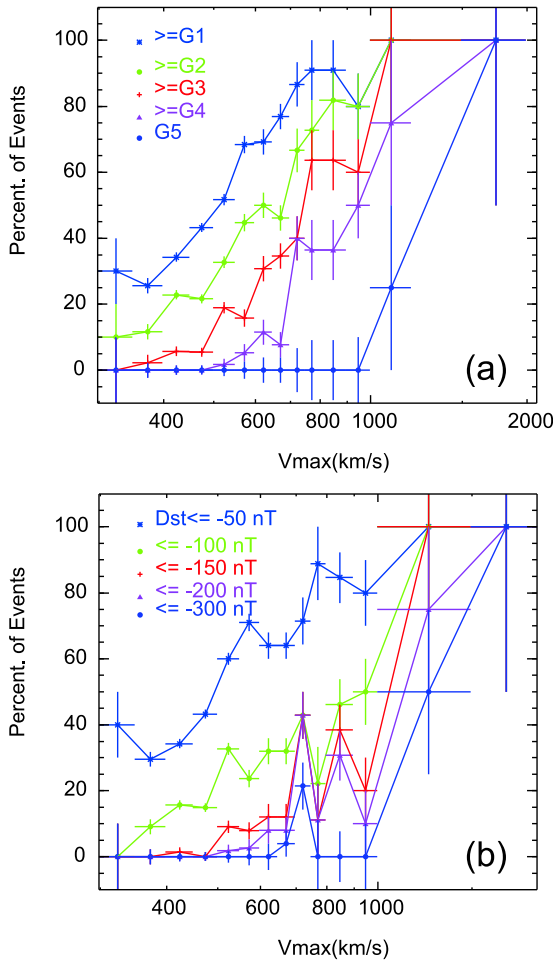

Figure 8. (a) Probability of occurrence of a storm equal to or exceeding NOAA size G1 to G5 versus maximum solar wind speed in the ICME or sheath based on events in 1996–2009. The "error bars" indicate the effect of changing the number of events by one. (b) Probability of occurrence of a storm exceeding various *Dst* thresholds versus maximum solar wind speed in the ICME or sheath.

on *Kp*. Specifically, G1 ("minor"): *Kp* = 5; G2 ("moderate"): *Kp* = 6; G3 ("strong"): *Kp* = 7; G4 ("severe"): *Kp* = 8 including a 9$^-$ and G5 ("extreme"): *Kp* = 9. Figure 6a shows results for the 1996–2009 ICMEs. The results suggest that for example, for an ICME with maximum E_y = 6 mV/m, there is a 100% probability that a ≥G1 storm will result, 90% for a ≥G2 storm, ~30% for a ≥G3 storm, <5% for a ≥G4 storm, and no chance of a G5 storm. The 50% probabilities lie at: E_y ~ 3.5 mV/m for ≥G1; E_y ~ 4.5 mV/m for ≥G2; E_y ~ 8 mV/m for ≥G3; and E_y ~ 12 mV/m for ≥G4. The value for G5 storms is difficult to estimate given the small number of such storms (Figure 6a, top), but may lie at E_y ~ 30–40 mV/m. To increase the sample of events with stronger geomagnetic activity, Figure 6b includes 34 pre-1996 ICMEs with E_y ≥ 10 mV/m. These were identified by examining solar wind magnetic field and plasma observations in the vicinity of intervals with E_y ≥ 10 mV/m for evidence of ICMEs and with reference to ICME/magnetic cloud related studies by ourselves and others [e.g., *Burlaga et al.*, 1987; *Lepping et al.*, 1990; *Richardson and Cane*, 1993, 1995; *Cane et al.*, 1996, and references therein]. However, the results are essentially unchanged and the number of the most geoeffective events is not significantly increased.

2.3. Geoeffectiveness and ICME Speed

[12] The results discussed so far again demonstrate that measuring E_y and/or B_s in the ICME and sheath using an upstream monitor such as ACE provides an excellent indication of the likely level of geomagnetic activity that will result. However, such a monitor provides little warning of impending activity, around an hour or less in the case of a spacecraft at L1 such as ACE. Halo CMEs directed toward the Earth may provide around 1 to 4 days advance warning of the possible arrival of an ICME at the Earth, but it is well established that only a subset of such CMEs are followed by geomagnetic storms [e.g., *St. Cyr et al.*, 2000; *Wang et al.*, 2002; *Zhao and Webb*, 2003; *Kim et al.*, 2005; *Moon et al.*, 2005] depending, for example, on the geoeffectiveness of the related ICME and whether this ICME actually encounters the Earth. An additional complication is that a large subset (almost a half) of near-Earth ICMEs in cycle 23 were not preceded by plausibly associated full or partial halo CMEs [*Cane and Richardson*, 2003; *Richardson and Cane*, 2010] including a few cases that generated intense storms [*Zhang et al.*, 2007].

[13] Figure 7a shows the maximum value of *Kp**10 plotted versus the plane of the sky speed of the halo or partial halo CME associated with the near-Earth ICMEs where this can be identified [*Richardson and Cane*, 2010] (the CME observations are from the LASCO coronagraphs on SOHO). Although the most severe (*Kp**10 ≥ 80) storms tend to be associated with the fastest CMEs [e.g., *Srivastava and Venkatakrishnan*, 2004] overall there is little correlation between CME speed and the maximum value of *Kp* associated with passage of the related ICME (*cc* = 0.296). Thus, even for those cases where the ICME associated with a halo or partial CME does encounter the Earth, the plane of the sky CME speed near the Sun is overall a poor predictor of geoeffectiveness.

[14] Figure 7b shows *Kp**10 plotted against the maximum solar wind speed measured in the sheath or ICME (V_{max}), while 7(c) shows the *Kp**10 versus the 1 AU transit speed of the leading edge of the ICME-related disturbance, i.e., the shock for a fast ICME. The correlations between *Kp* and V_{max} or the 1 AU transit speed are stronger than with the halo or partial halo CME speed though still modest (*cc* = 0.584 or *cc* = 0.576, respectively). Hence, using just the ICME speed, it is unlikely that the geoeffectiveness of a particular ICME or sheath can accurately predicted. Instead, this large sample of events may be used to estimate the probability of certain levels of geoeffectiveness based on the ICME speed. Figure 8a shows the probability of exceeding particular G storm sizes as a function of V_{max}. For example, for a

maximum solar wind speed in the ICME or sheath of 600 km/s, there is a ~70% probability of a ≥G1 storm, ~50% probability of a ≥G2 storm, ~20% probability of a ≥G3 storm, ~5% probability of a ≥G4 storm, and ~0% probability of a G5 storm. A 50% probability of a particular size storm or larger occurs at V_{max} ~ 500 km/s for G1, 600 km/s for G2, 750 km/s for G3, 1000 km/s for G4, and 1300 km/s for G5, though this last result is compromised by the limited number of G5 storms in our sample; here the "error bars" indicate the effect of changing the number of events by one.

[15] Figure 8b shows the probability of *Dst* exceeding specified thresholds as a function of V_{max}, again indicating a generally increased likelihood of stronger storms as the maximum speeds in the ICME or sheath increase. A 50% probability of a *Dst* ≤ −50 nT storm occurs at V_{max} ~ 500 km/s, and at around 900 km/s for *Dst* ≤ −100 nT. For larger storm thresholds, the curves are closely spaced, so it would be difficult to assess the probability of such storms occurring based on V_{max}, though it is evident that above V_{max} ~ 1000 km/s, activity is likely to exceed *Dst* = −150 nT, and there is a 50% or higher probability of exceeding *Dst* = −300 nT.

3. Summary and Discussion

[16] We have summarized the geoeffectiveness (*Dst* and *Kp*) of the over 300 ICMEs that passed the Earth during 1996–2009, encompassing solar cycle 23 [*Richardson and Cane*, 2010]. Our results demonstrate, as have previous studies, that the geoeffectiveness is strongly correlated with B_s and E_y in the ICME or sheath, suggesting that observations of the solar wind B_s and E_y upstream of the Earth may provide reliable estimates of the potential geoeffectiveness of ICMEs and their related sheaths. We have not explicitly considered here the duration over which these conditions prevail, but this is also important, as incorporated for example into empirical prediction methods (e.g., *O'Brien and McPherron* [2000] for *Dst*). The ICME speed, whether measured in situ, or based on the 1 AU transit time, has a weaker correlation with geoeffectiveness and hence cannot be used to give a reliable prediction for a specific event. However, using this large sample of ICMEs, we can estimate the probability that a particular storm threshold will be attained or exceeded as a function of ICME speed.

[17] The results may be of interest in a scenario where ICMEs approaching the Earth can be identified remotely, for example using coronagraph observations from spacecraft separated in heliolongitude from the Earth (such as the STEREO spacecraft [e.g., *Thernisien et al.*, 2009; *Liu et al.*, 2010]), and all-sky imagers such as the Solar Mass Ejection Imager (SMEI) [e.g., *Howard et al.*, 2006; *Webb et al.*, 2006]. Our overall results (Figure 1) suggest that only around one in four of these ICMEs is likely to generate an intense (*Dst* ≤ −100 nT) storm, while a severe (*Dst* ≤ −200 nT) storm will result for around one in sixteen events. Thus, if a storm warming were to be issued on the approach of any ICME, there would be many "false alarms." Identifying a method of distinguishing potentially geoeffective ICMEs might improve the situation. Current remote sensing observations provide no direct information on either the magnitude or direction of the magnetic field within the ICME and sheath that are evidently the major factors controlling the geoeffectiveness of the ICME. (We note though that *Wood and Howard* [2009] have used STEREO coronagraph observations to infer the orientation of a flux rope structure within a CME which may be a promising technique to predict the field configuration in an ICME.) The speed of the ICME may be determined more readily. However, the results presented above demonstrate that the ICME speed is a less reliable predictor of geoeffectiveness. Nevertheless, we suggest that the results in Figure 8 could be used in conjunction with remote sensing estimates of the speeds of ICMEs approaching the Earth to help indicate the potential geoeffectiveness of these ICMEs. For example, for an ICME approaching at 600 km/s, these results suggest, as noted above, that there is a ~70% probability of a ≥G1 storm, 50% of a ≥G2, 20% of a ≥G3, 5% of a G4 and 0%of a G5. Considering *Dst*, there is a ~70% probability of *Dst* ≤ −50 nT, 30% of *Dst* ≤ −100 nT, 10% of *Dst* ≤ −150 nT and 5% of *Dst* ≤ −200 nT.

[18] As an illustration, *Liu et al.* [2010] used STEREO observations to reconstruct the trajectories of two ICMEs that passed the Earth, both also noted by *Richardson and Cane* [2010]. The first ICME and the related shock passed the Earth on November 19–20, 2007. *Liu et al.* [2010] estimated the ICME speed from remote sensing to be 388 km/s (Feature 2 in their Table 1). This ICME was associated with minimum (provisional) *Dst* = −63 nT, and maximum *Kp**10 = 53, i.e., $Kp = 5^+$, corresponding to a G1 storm. Figure 8a suggests a 30% probability of a G1 storm and 10% for a G2 storm with this ICME speed. We note that V_{max} measured in situ was higher (~ 500 km/s) which would raise the probability of a G1 storm to ~ 40%. Figure 8b suggests a ~30% probability of *Dst* ≤ −50 nT for a speed of 388 km/s.

[19] The second ICME considered by *Liu et al.* [2010] [see also *Davis et al.*, 2009] passed the Earth on December 17, 2008. The associated disturbance, possibly a developing shock, arrived at ~12 UT on December 16 [*Richardson and Cane*, 2010]. The estimated ICME speed from remote sensing was ~400 km/s [cf. *Liu et al.*, 2010, Figure 9] (in situ V_{max} was ~380 km/s). The ICME was associated with minimum (quick-look) *Dst* = −18 nT and maximum *Kp**10 = 27, i.e., $Kp = 3^-$, so the G1 storm threshold was not reached. For a speed of 400 km/s, our results suggest a 30% chance of a G1 storm or *Dst* ≤ −50 nT.

[20] In another study, *Davis et al.* [2011] inferred speeds of 469 to 545 km/s for an Earthward directed CME on April 8, 2010 using STEREO coronagraph observations and various analysis methods. The associated ICME reached the Earth on April 11–12 and was accompanied by geomagnetic activity with minimum *Dst* = −56 nT and $Kp = 6^-$, i.e., a G2 storm. Figure 8a suggests a ~50% probability of a ≥G1 storm, ~30% for ≥G2, and ~10% for ≥G3 for such speeds, so the observed G2 storm is in line with such predictions.

Figure 8b suggests a ~50% probability of $Dst < -50$ nT, and ~20% for $Dst < -100$ nT, again consistent with the observed *Dst*. Overall, the observed geoeffectiveness of these three remotely sensed ICMEs is reasonably consistent with the expectations based on the results obtained using our large sample of ICMEs. In particular, these results suggest that the ICMEs are unlikely to be associated with particularly strong storms.

[21] While combining remote sensing of earth-directed ICMEs and the results in this study may be a useful technique for forecasting potential geoeffectiveness of ICMEs, there are a few points to note. In particular, a significant fraction of major geomagnetic storms involve the interaction of more than one ICME and/or the related shocks, or an ICME interaction with a corotating high-speed stream [e.g., *Burlaga et al.*, 1987; *Farrugia et al.*, 2006a, 2006b; *Zhang et al.*, 2007]. Thus, the geoeffectiveness of an ICME approaching the Earth may be influenced by the structures in the vicinity of the ICME. In addition, as noted above, there are limited in situ observations at the times of the largest geomagnetic storms, and few such storms, so it is difficult to estimate the probability of such important storms occurring based on the limited statistics. Extending our analysis to events from earlier solar cycles will increase the number of events that may be included, as in Figure 6b, though the problem of the small number of exceptionally geoeffective ICMEs is likely to remain.

[22] Another aspect is whether the potential geoeffectiveness of an ICME with a particular speed is influenced by, for example, the phase of the solar cycle (e.g., the fraction of ICMEs that are magnetic clouds, and hence potentially more geoeffective, may be larger at solar minimum [*Richardson and Cane*, 2004]) or the time of the year (in particular, geomagnetic activity tends to be enhanced around the equinoxes compared to the solstices [e.g., *Russell and McPherron*, 1973; *Cliver et al.*, 2000; *Zhang et al.*, 2007]). Investigation of the latter effect suggests that there is only a slight dependence on whether the ICME occurs closer to the solstice or the equinox. For example, the probability of a 400–500 km/s ICME generating a G1 storm is 35% for ICMEs closer to solstice compared with 45% for those closer to equinox, while at 500–600 km/s, the probabilities are 56% and 62%, respectively. A larger set of events is required to allow the variation in geoeffectiveness with time of year to be investigated more fully, especially for the stronger storms.

[23] We have also not separated magnetic clouds and other ICMEs in the results in Figure 8. However, since magnetic clouds are typically more geoeffective, identification of a flux rope structure in the CME/ICME by remote sensing [e.g., *Wood and Howard*, 2009] might be a reason to increase the expected geoeffectiveness. On the other hand, it is possible that *every* ICME includes a flux rope substructure that in principle might be identified remotely, but this only encounters the Earth in a subset (around 25%) of ICMEs that we then identify as "magnetic clouds," in which case the statistics in Figure 8 naturally allow for this situation.

[24] **Acknowledgments.** The ACE data sets used in this study were provided by the ACE Science Center (http://www.srl.caltech.edu/ACE/ASC/). The OMNI solar wind database, compiled by the Space Physics Data Facility at the Goddard Space Flight Center, is available at http://omniweb.gsfc.nasa.gov/.

References

Bartels, J., N. H. Heck, and H. F. Johnston (1939), The three-hour range index measuring geomagnetic activity, *J. Geophys. Res.*, *44*, 411.

Burlaga, L. F., K. W. Behannon, and L. W. Klein (1987), Compound streams, magnetic clouds and major geomagnetic storms, *J. Geophys. Res.*, *92*, 5725.

Cane, H. V., and I. G. Richardson (2003), Interplanetary coronal mass ejections in the near-Earth solar wind during 1996–2002, *J. Geophys. Res.*, *108*(A4), 1156, doi:10.1029/2002JA009817.

Cane, H. V., I. G. Richardson, and T. T. von Rosenvinge (1996), Cosmic ray decreases: 1964–1994, *J. Geophys. Res.*, *101*, 21,561.

Cliver, E. W., Y. Kamide, and A. G. Ling (2000), Mountains versus valleys: Semiannual variation of geomagnetic activity, *J. Geophys. Res.*, *105*, 2413.

Davis, C. J., J. A. Davies, M. Lockwood, A. P. Rouillard, C. J. Eyles, and R. A. Harrison (2009), Stereoscopic imaging of an Earth-impacting solar coronal mass ejection: A major milestone for the STEREO mission, *Geophys. Res. Lett.*, *36*, L08102, doi:10.1029/2009GL038021.

Davis, C. J., et al. (2011), A comparison of space weather analysis techniques used to predict the arrival of the Earth-directed CME and its shockwave launched on 8 April 2010, *Space Weather*, *9*, S01005, doi:10.1029/2010SW000620.

Dungey, J. R. (1961), Interplanetary magnetic field and auroral zones, *Phys. Rev. Lett.*, *6*, 47.

Echer, E., W. D. Gonzalez, B. T. Tsurutani, and A. L. C. Gonzalez (2008), Interplanetary conditions causing intense geomagnetic storms ($Dst \le -100$ nT) during solar cycle 23 (1996–2006), *J. Geophys. Res.*, *113*, A05221, doi:10.1029/2007JA012744.

Farrugia, C. J., L. F. Burlaga, and R. P. Lepping (1997), Magnetic clouds and the quiet/storm effect at Earth: A review, in *Magnetic Storms*, *Geophys. Monogr. Ser.*, vol. 98, edited by B. T. Tsurutani et al., p. 91, AGU, Washington, D. C.

Farrugia, C. J., et al. (1998), Geoeffectiveness of three WIND magnetic clouds: A comparative study, *J. Geophys. Res.*, *103*, 17,261.

Farrugia, C. J., H. Matsui, H. Kucharek, V. K. Jordanova, R. B. Torbert, K. W. Ogilvie, D. B. Berdichevsky, C. W. Smith, and R. Skoug (2006a), Survey of intense Sun-Earth connection events (1995–2003), *Adv. Space. Res.*, *38*(3), 498.

Farrugia, C. J., V. K. Jordanova, M. F. Thomsen, G. Lu, S. W. H. Cowley, and K. W. Ogilvie (2006b), A two-ejecta event associated with a two-step geomagnetic storm, *J. Geophys. Res.*, *111*, A11104, doi:10.1029/2006JA011893.

Gonzalez, W. D., and B. T. Tsurutani (1987), Criteria of interplanetary parameters causing intense magnetic storms ($D_{st} < -100$ nT), *Planet. Space. Sci.*, *35*, 1101.

Gopalswamy, N., S. Akiyama, S. Yashiro, G. Michalek, and R. P. Lepping (2008), Solar sources and geospace consequences of interplanetary magnetic clouds observed during solar cycle 23, *J. Atmos. Sol. Terr. Phys.*, *70*, 245.

Gosling, J. T. (1990), Coronal mass ejections and magnetic flux ropes in interplanetary space, in *Physics of Magnetic Flux Ropes*, *Geophys. Monogr. Ser.*, vol. 58, edited by C. T. Russell, E. R. Priest, and L. C. Lee, p. 343, AGU, Washington, D. C.

Gosling, J. T., D. J. McComas, J. L. Phillips, and S. J. Bame (1991), Geomagnetic activity associated with Earth passage of interplanetary shock disturbances and coronal mass ejections, *J. Geophys. Res.*, *96*, 7831.

Howard, T. A., D. F. Webb, S. J. Tappin, D. R. Mizuno, and J. C. Johnston (2006), Tracking halo coronal mass ejections from 0–1 AU and space weather forecasting using the Solar Mass Ejection Imager (SMEI), *J. Geophys. Res.*, *111*, A04105, doi:10.1029/2005JA011349.

Huttunen, K., and H. Koskinen (2004), Importance of post-shock streams and sheath region as drivers of intense magnetospheric storms and high- latitude activity, *Ann. Geophys.*, *22*, 1729.

Huttunen, K. E. J., R. Schwenn, V. Bothmer, and H. E. J. Koskinen (2005), Properties and geoeffectiveness of magnetic clouds in the rising, maximum and early declining phases of solar cycle 23, *Ann. Geophys.*, *23*, 625.

Ji, E.-Y., Y.-J. Moon, K.-H. Kim, and D.-H. Lee (2010), Statistical comparison of interplanetary conditions causing intense geomagnetic storms ($Dst \leq -100$ nT), *J. Geophys. Res.*, *115*, A10232, doi:10.1029/2009JA015112.

Kane, R. P. (2005), How good is the relationship of solar and interplanetary plasma parameters with geomagnetic storms?, *J. Geophys. Res.*, *110*, A02213, doi:10.1029/2004JA010799.

Kim, R.-S., K.-S. Cho, Y.-J. Moon, Y.-H. Kim, Y. Yi, M. Dryer, S.-C. Bong, and Y.-D. Park (2005), Forecast evaluation of the coronal mass ejection (CME) geoeffectiveness using halo CMEs from 1997 to 2003, *J. Geophys. Res.*, *110*, A11104, doi:10.1029/2005JA011218.

Klein, L. W., and L. F. Burlaga (1982), Interplanetary magnetic clouds at 1 AU, *J. Geophys. Res.*, *87*, 613.

Lepping, R. P., J. A. Jones, and L. F. Burlaga (1990), Magnetic field structure of interplanetary magnetic clouds at 1 AU, *J. Geophys. Res.*, *95*, 11,957.

Lepping, R. P., D. B. Berdichevsky, C.-C. Wu, A. Szabo, T. Narock, F. Mariani, A. J. Lazarus, and A. J. Quivers (2006), A summary of WIND magnetic clouds for years 1995–2003: Model-fitted parameters, associated errors and classifications, *Ann. Geophys.*, *24*, 215.

Liu, Y., A. Thernisien, J. G. Luhmann, A. Vourlidas, J. A. Davies, R. P. Lin, and S. D. Bale (2010), Reconstructing coronal mass ejections with coordinated imaging and in situ observations: Global structure, kinematics, and implications for space weather forecasting, *Astrophys. J.*, *722*, 1762.

Mayaud, P. N. (1980), *Derivation, Meaning, and Use of Geomagnetic Indices*, *Geophys. Monogr. Ser.*, vol. 22, AGU, Washington, D. C.

Menvielle, M., and A. Berthelier (1991), The *K*-derived planetary indices: Description and availability, *Rev. Geophys.*, *29*(3), 415, doi:10.1029/91RG00994.

Moon, Y.-J., K.-S. Cho, M. Dryer, Y.-H. Kim, S.-C. Bong, J. Chae, and Y. D. Park (2005), New geoeffective parameters of very fast halo coronal mass ejections, *Astrophys. J.*, *624*, 414.

Neugebauer, M., and R. Goldstein (1997), Particle and field signatures of coronal mass ejections in the solar wind, in *Coronal Mass Ejections*, *Geophys. Monogr. Ser.*, vol. 99, edited by N. Crooker, J. A. Joselyn, and J. Feynman, p. 245, AGU, Washington, D. C.

O'Brien, T. P., and R. L. McPherron (2000), An empirical phase space analysis of ring current dynamics: Solar wind control of injection and decay, *J. Geophys. Res.*, *105*, 7707.

Richardson, I. G., and H. V. Cane (1993), Signatures of shock drivers in the solar wind and their dependence on the solar source location, *J. Geophys. Res.*, *98*, 15,295.

Richardson, I. G., and H. V. Cane (1995), Regions of abnormally low proton temperature in the solar wind (1965–1991) and their association with ejecta, *J. Geophys. Res.*, *100*, 23,397.

Richardson, I. G., and H. V. Cane (2004), The fraction of interplanetary coronal mass ejections that are magnetic clouds: Evidence for a solar cycle variation, *Geophys. Res. Lett.*, *31*, L18804, doi:10.1029/2004GL020958.

Richardson, I. G., and H. V. Cane (2010), Near-Earth interplanetary coronal mass ejections during solar cycle 23 (1996–2009): Catalog and summary of properties, *Sol. Phys.*, *264*, 189.

Richardson, I. G., and J. Zhang (2008), Multiple-step geomagnetic storms and their interplanetary drivers, *Geophys. Res. Lett.*, *35*, L06S07, doi:10.1029/2007GL032025.

Richardson, I. G., E. W. Cliver, and H. V. Cane (2001), Sources of geomagnetic storms for solar minimum and maximum conditions during 1972–2000, *Geophys. Res. Lett.*, *28*, 2569.

Rostoker, G. (1972), Geomagnetic indices, *Rev. Geophys.*, *10*(4), 935, doi:10.1029/RG010i004p00935.

Russell, C. T., and R. L. McPherron (1973), Semiannual variation of geomagnetic activity, *J. Geophys. Res.*, *78*, 92.

Srivastava, N., and P. Venkatakrishnan (2004), Solar and interplanetary sources of major geomagnetic storms during 1996–2002, *J. Geophys. Res.*, *109*, A10103, doi:10.1029/2003JA010175.

St. Cyr, O. C., et al. (2000), Properties of coronal mass ejections: SOHO LASCO observations from January 1996 to June 1998, *J. Geophys. Res.*, *105*, 18,169.

Sugiura, M. (1964), Hourly values of equatorial *Dst* for the IGY, *Ann. Int. Geophys. Year*, *35*, 9.

Thernisien, A., A. Vourlidas, and R. A. Howard (2009), Forward modeling of coronal mass ejections using STEREO/SECCHI data, *Sol. Phys.*, *256*, 111.

Tsurutani, B. T., and W. D. Gonzalez (1997), The interplanetary causes of magnetic storms: A review, in *Magnetic Storms*, *Geophys. Monogr. Ser.*, vol. 98, edited by B. T. Tsurutani et al., p. 77, AGU, Washington, D. C.

Tsurutani, B. T., E. J. Smith, W. D. Gonzalez, F. Tang, and S. I. Akasofu (1988), Origin of interplanetary southward magnetic fields responsible for major magnetic storms near solar maximum (1978–1979), *J. Geophys. Res.*, *93*, 8519.

Wang, Y. M., P. Z. Ye, S. Wang, G. P. Zhou, and J. X. Wang (2002), A statistical study on the geoeffectiveness of Earth-directed coronal mass ejections from March 1997 to December 2000, *J. Geophys. Res.*, *107*(A11), 1340, doi:10.1029/2002JA009244.

Webb, D. F., et al. (2006), Solar Mass Ejection Imager (SMEI) observations of coronal mass ejections (CMEs) in the heliosphere, *J. Geophys. Res.*, *111*, A12101, doi:10.1029/2006JA011655.

Wood, B. E., and R. A. Howard (2009), An empirical reconstruction of the 2008 April 26 coronal mass ejection, *Astrophys. J.*, *702*, 901.

Wu, C.-C., and R. P. Lepping (2007), Comparison of the characteristics of magnetic clouds and magnetic cloud-like structures for the events of 1995–2003, *Sol. Phys.*, *242*, 159.

Zhang, G., and L. F. Burlaga (1988), Magnetic clouds, geomagnetic disturbances, and cosmic ray decreases, *J. Geophys. Res.*, *93*, 2511.

Zhang, J., et al. (2007), Solar and interplanetary sources of major geomagnetic storms ($Dst \leq -100$ nT) in 1996–2005, *J. Geophys. Res.*, *112*, A10102, doi:10.1029/2007JA012321.

Zhang, J., I. G. Richardson, and D. F. Webb (2008), Interplanetary origin of multiple-dip geomagnetic storms, *J. Geophys. Res.*, *113*, A00A12, doi:10.1029/2008JA013228.

Zhao, X. P., and D. F. Webb (2003), Source regions and storm effectiveness of frontside full halo coronal mass ejections, *J. Geophys. Res.*, *108*(A6), 1234, doi:10.1029/2002JA009606.

Zurbuchen, T. H., and I. G. Richardson (2006), In-situ solar wind and magnetic field signatures of interplanetary coronal mass ejections, *Space Sci. Rev.*, *123*, 31.

H. V. Cane and I. G. Richardson, Astroparticle Physics Laboratory, Code 661, NASA Goddard Space Flight Center, Greenbelt, MD 20771, USA. (hilary.cane@utas.edu.au; ian.g.richardson@nasa.gov)